The Mantle Transition Zone in Fennoscandia: Enigmatic High Topography Without Deep Mantle Thermal Anomaly

Anna Makushkina, Benoit Tauzin, Hrjoje Tkalcic, Hans Thybo

AGU100 ADVANCING EARTH AND SPACE SCIENCE

Geophysical Research Letters

RESEARCH LETTER
10.1029/2018GL081742

Key Points:
- The average mantle transition zone thickness beneath Fennoscandia, 242 +/- 12 km, is close to the global standard thickness
- There is no evidence for deep active geodynamic processes in the region as a support for the high topography in western Fennoscandia
- Upper mantle seismic velocities are fast relative to the spherically symmetric Earth model IASP91

Supporting Information:
- Supporting Information S1
- Data Set S1
- Data Set S2

Correspondence to:
A. Makushkina,
anna.makushkina@anu.edu.au

Citation:
Makushkina, A., Tauzin, B., Tkalčić, H., & Thybo, H. (2019). The mantle transition zone in Fennoscandia: Enigmatic high topography without deep mantle thermal anomaly. *Geophysical Research Letters*, *46*, 3652–3662. https://doi.org/10.1029/2018GL081742

Received 18 DEC 2018
Accepted 11 MAR 2019
Accepted article online 15 MAR 2019
Published online 2 APR 2019

The Mantle Transition Zone in Fennoscandia: Enigmatic High Topography Without Deep Mantle Thermal Anomaly

Anna Makushkina[1], Benoît Tauzin[1,2], Hrvoje Tkalčić[1], and Hans Thybo[3,4,5]

[1]Research School of Earth Sciences, The Australian National University, Canberra, ACT, Australia, [2]Université de Lyon, UCBL, ENS Lyon, CNRS, Laboratoire de Géologie de Lyon, Terre, Planètes, Environnement, Villeurbanne, France, [3]Eurasia Institute of Earth Sciences, Istanbul Technical University, Istanbul, Turkey, [4]School of Earth Sciences, China University of Geosciences, Wuhan, China, [5]Center for Earth Evolution and Dynamics (CEED), University of Oslo, Oslo, Norway

Abstract Seismological data acquired by dense receiver networks in Fennoscandia enable imaging of Earth's upper mantle structure at unprecedented resolution and provide critical observations for resolving the ongoing debate on the cause of enigmatic high topography in Norway. Proposed mechanisms for the high topography include impact of a mantle plume, as supported by the observation of low seismic velocities in the uppermost mantle in southern Norway in contrast to high velocities in Sweden. We image the mantle transition zone (MTZ) in Fennoscandia by common conversion point stacking of 14,873 receiver functions from 14 networks including the recently deployed ScanArray. We find both MTZ discontinuities at their expected depths of 410 and 660 km within an uncertainty of 5–15 km and the thickness of the MTZ similar to the global average. These observations show that the high topography in western Scandinavia cannot be caused by thermal influence from the deep mantle.

Plain Language Summary High mountains in Norway have long puzzled scientists because it is challenging to explain their existence. Numerous explanations have been proposed including processes deep inside the Earth. Our results show that these processes must be located above 410-km depth. This observation is critical for the ongoing debate on the cause of the enigmatic mountains in Scandinavia. New data acquired between 2012 and 2017 by the collaborative ScanArray project between European institutions allow mapping of the mantle transition zone—the deepest layer possibly involved in the mountain support. We show that the mantle transition zone boundaries beneath Fennoscandia are close to reference depths and the zone has a standard thickness. As the depths to these boundaries are sensitive to temperatures, this indicates that the mantle transition zone in this area is unaffected by any ongoing deep process. Therefore, the explanation for the high topography in Norway must be found above the mantle transition zone. This study provides the first map of the mantle transition zone below Fennoscandia, which will be valuable for any further global studies of the mantle transition zone.

1. Introduction

The Baltic Shield (Fennoscandia) is the tectonically quiet northwestern part of the East European Craton. The opening of the North Atlantic Ocean in the Early Cenozoic was the last tectonic event that affected this region by creating a wide passive margin offshore western Norway. Current topography of Norway is generally high with two domes higher than 1,500 m in the southern and northern parts and peak altitude up to 2,469 m (Figure 1a). This high topography remains enigmatic and is vividly debated (cf. Anell et al., 2009; Japsen & Chalmers, 2000). The debate has centered on the role of the Caledonian orogeny (Gee et al., 2008; Figure 1b), which affected Fennoscandia and terminated around 400 Ma, as well as the influence of accelerated recent onshore erosion over the latest 5 Myr (Anell et al., 2010). One point of view (Nielsen et al., 2009; Pedersen et al., 2016) explains the present high topography by the interplay between erosion and isostatic rebound since Caledonian time, while the other point of view (Anell et al., 2012; Gabrielsen et al., 2010; Japsen et al., 2012) implies that additional geodynamic processes are responsible for the recent uplift of the Scandinavian mountains during the Cenozoic.

It has been hypothesized that effects of the Icelandic hotspot could explain the high elevations by creating positive buoyancy of the upper mantle (UM) due to high temperature. A low-velocity zone (LVZ) in the

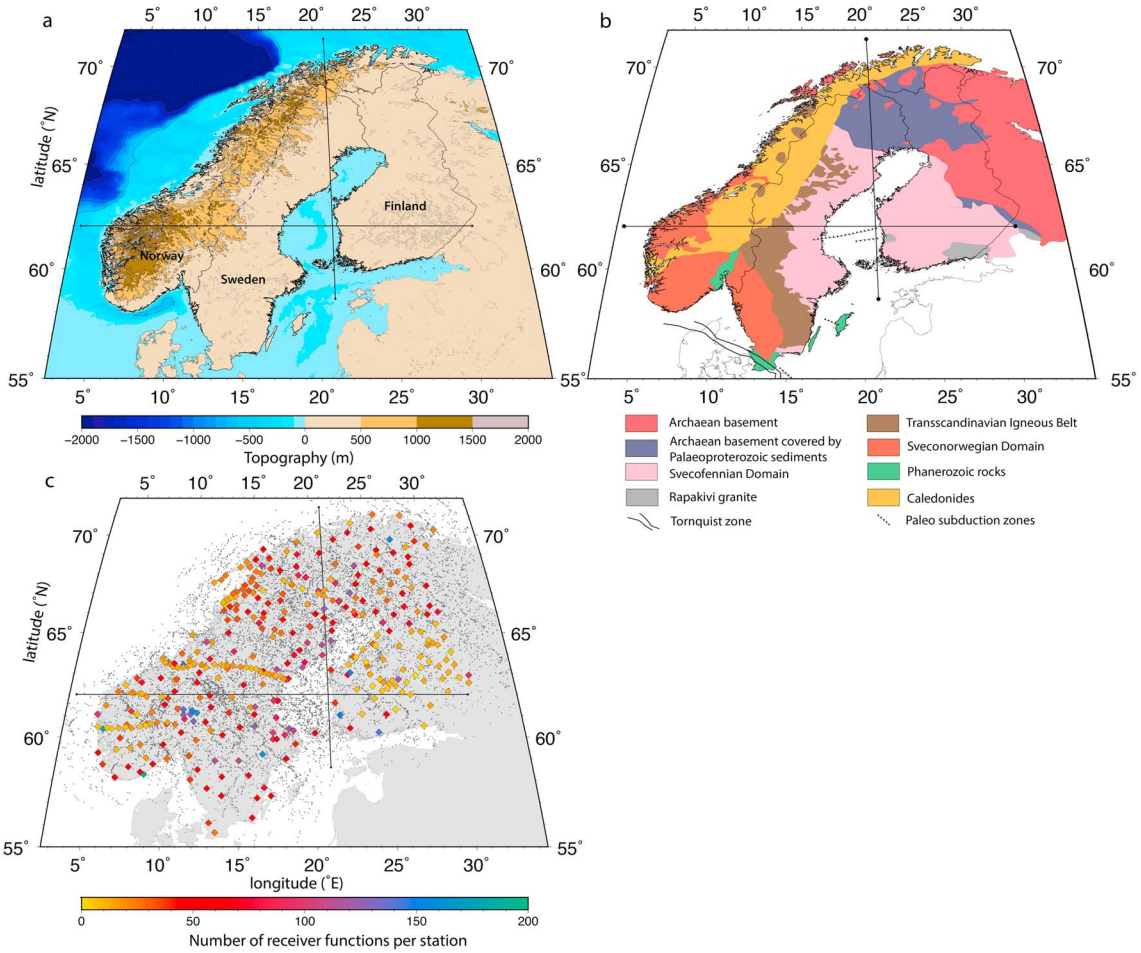

Figure 1. (a) Topography map of the study area outlining areas of high topography with contours at 500, 1,000, 1,500, and 2,000 m. High topography are generally only found in Caledonian deformed areas as outlined by dashed dark blue line. (b) Generalized geological map (after Högdahl et al., 2004) of Fennoscandia. Locations of the Sorgenfrei-Tornquist zone and paleo subduction zones are after Korja and Heikkinen (2005). Political boundaries are shown with solid black lines in (a) and (b) maps. (c) Map of seismic stations used and coverage by *P*-to-*S* piercing points at the mantle transition zone depth in Fennoscandia. Stations are shown as diamond symbols with color according to number of receiver functions used to produce maps. Small dark gray circles correspond to piercing points at 535-km depth. Black lines indicate locations of two seismic profiles shown in Figure 2.

UM observed below Southern Norway in tomography images (Medhus et al., 2012; Rickers et al., 2013; Wawerzinek et al., 2013) has been interpreted as a finger of the proposed Icelandic mantle plume (Schoonman et al., 2017). However, due to poor resolution of seismic body wave tomographic images (Foulger et al., 2013), the vertical extent of the LVZ is not completely resolved (Medhus et al., 2012; Wawerzinek et al., 2013), and full-waveform tomography models image it differently (Rickers et al., 2013; Zhu et al., 2015). As such, there is currently no clear indication whether the LVZ extends to mantle transition zone (MTZ) depths and temperature anomalies affect mineralogical phase changes.

The MTZ is characterized by abrupt increase of seismic velocity across its two boundaries located approximately at 410- and 660-km depths. Mineral physics experiments indicate that the major contributors to these boundaries are phase changes of olivine into wadsleyite at 410 km, and ringwoodite into perovskite + ferropericlase at 660-km depth (Ringwood, 1969). These mineral phase changes are temperature and pressure dependent, and the thickness of the MTZ may provide information on the temperature due to the opposite sign of the Clapeyron slopes for the two reactions (Bina & Helffrich, 1994). Assuming homogeneous composition, we expect that the MTZ is thicker than normal at low temperature and thinner than normal at high temperature. Measurement of the MTZ thickness therefore allows the detection of temperature anomalies that originate deep in the mantle and thereby constrains possible underlying local geodynamical processes. However, this ideal picture may be complicated by several effects. UM velocity anomalies may shift the

apparent depths of discontinuities and introduce a positive correlation that is opposite to the temperature effect (e.g., Tauzin & Ricard, 2014). Additionally, the presence of minerals other than olivine may change the Clapeyron slopes of the phase changes (Irifune, 1987). Finally, the presence of volatile elements potentially affects the MTZ by reducing seismic velocities, shifting the depth of phase transitions (Thio et al., 2016), broadening the discontinuities (Frost, 2003; Wood, 1995), and triggering partial melting (Bercovici & Karato, 2003).

Global studies (Lawrence & Shearer, 2006a; Tauzin et al., 2008) of the MTZ thickness have used data from two stations in Fennoscandia located in the very north (KEV) and south (KONO). These and other regional-scale receiver functions (RFs) studies (Alinaghi et al., 2003; Bock et al., 2001; Kozlovskaya et al., 2008; Vinnik et al., 2016) show that *P*-to-*S* conversion signals for the 410- and 660-km discontinuities ("410" and "660" in the following text) arrive up to 2 s earlier than the standard times in the IASP91 model in Finland (Kozlovskaya et al., 2008) and Sweden (Olsson et al., 2007; Vinnik et al., 2016). This was explained by higher velocities in the UM than in the IASP91 model.

Here we present new maps of the MTZ characteristics in terms of depths to the 410 and 660 and the MTZ thickness. These maps are obtained from common conversion point (CCP) stacks of 14,873 teleseismic RFs for 398 stations distributed across Fennoscandia. These data include the recent ScanArray experiment (Thybo et al., 2012) conducted between 2012 and 2017 as a collaborative project between several European institutions. The new data allow imaging the deep structure in Fennoscandia at unprecedentedly high resolution (~200 km lateral, ~15 km vertical) to improve our understanding of the geodynamical processes currently acting in the region.

2. Data and Methods

2.1. Seismic Networks

We use data acquired by broadband recorders deployed during multiple seismic experiments in Fennoscandia (Figure 1c and Figure S1 in the supporting information). The core of our study is the newly acquired data from the ScanArray experiment (Thybo et al., 2012). The primary motivation for the ScanArray experiment is to enable the understanding of surface topography. In addition to ScanArray stations, we use other local permanent and temporary deployments. The full list of the 398 stations and 14 networks is provided in the supporting information (Figure S1 and Table S1). The spacing between stations is nominally 50 km, and it varies between 10 and 100 km.

2.2. Method

To map the depths to boundaries of the MTZ and its thickness, we use CCP stacking of *P* wave RFs (Dueker & Sheehan, 1997; Tauzin et al., 2013; Zhu, 2000). The RF method detects sharp changes in seismic velocities based on identification of *P*-to-*S* converted phases (Figure S1b). CCP stacking allows creation of depth-migrated images of the observed discontinuities. High data density is required to form robust images by stacking as the amplitudes of converted signals rarely exceed 5% of the *P* wave amplitude and are often at the level of the background noise.

We apply this technique to seismic records of 43,684 teleseismic events with magnitudes larger than 5.5 in the epicentral distance range 30–95° (Figure S1a). *P* wave RFs (e.g., Langston, 1979; Vinnik, 1977) were calculated for each event by deconvolving the radial by the vertical component seismogram filtered with a 0.5- to 20-s band pass. We applied iterative time domain deconvolution (Ligorría & Ammon, 1999) with a low-pass filter with Gaussian width $a = 1.0$. Subsequently, we calculated the piercing point locations at 535-km depth for each RF (Figure 1c) and the corresponding raypath using the IASP91 model. The absolute shear wave velocity value from a velocity model was attributed to each of the points along the raypaths for the migration and depth conversion. In this study we used the IASP91 1-D velocity model (Kennett & Engdahl, 1991) and the 3-D velocity model by Zhu et al. (2015, hereafter called ZHU15). The latter model has good coverage of Fennoscandia by use of more than 20 stations in Fennoscandia. The RFs were moveout-corrected according to ray parameter and velocity model in the spatial domain and projected onto profiles to form resulting 2-D CCP stacked images (Figures 2 and S2). Similar to Tauzin et al. (2013), Gaussian smoothing along the horizontal axis is applied to the images with a standard deviation of 50 km.

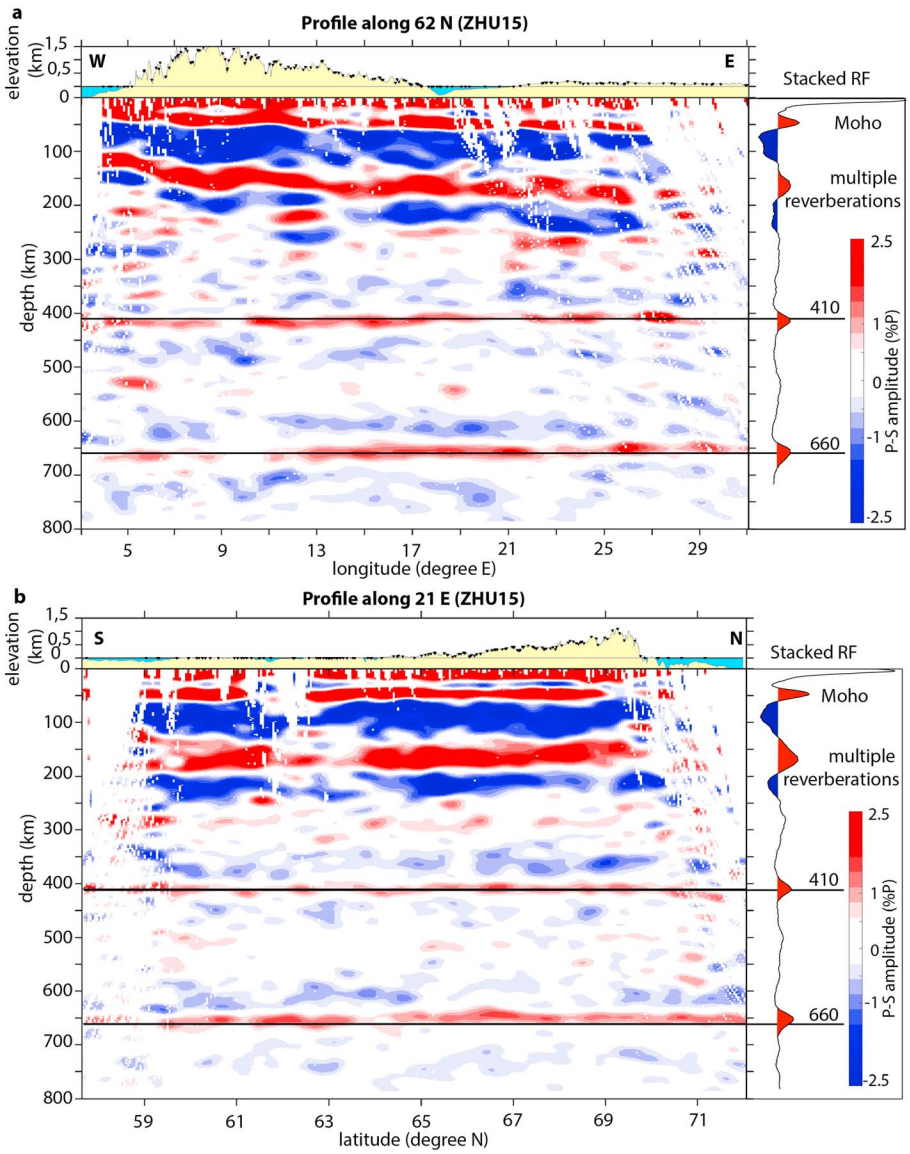

Figure 2. Common conversion point stacks of receiver functions, using the ZHU15 velocity model, along profiles located (a) 62°N and (b) 21°E; cf. Figure 1. Red color corresponds to converted signals from discontinuities with a downward positive gradient of shear velocities, and blue color corresponds to a decrease of velocity. Black solid horizontal lines at 410- and 660-km depths indicate reference depths for the mantle transition zone discontinuities. The upper panel of each profile shows topography (yellow = crust; blue = water) with station locations projected onto it (black dots). Right-hand diagrams show stacks of all the receiver functions (RFs) in the profiles.

We used stacks of RFs by networks to assess if the corresponding data have a reasonable signal-to-noise ratio (Figure S3).

Red signals in our images (Figures 2 and S2) correspond to positive amplitude and can be related to sharp downward increasing gradients of shear wave velocity. The maximum expected thickness for these gradients is less than $\lambda_P/2 \approx 50$ km (Bostock, 1999), where λ_P is the P wavelength at the dominant period (~10 s). Amplitudes in blue mark negative amplitudes associated with velocity decreases. Given the band pass of the RF data, the vertical resolution is ~15 km (given by the width of the Gaussian pulse in the depth domain at half the maximum amplitude).

Our CCP stacked profiles correspond to the projection of RFs with piercing points at 535-km depth and within 100 km from the profile. Thus, the obtained images have a lateral resolution of ~200 km. They are

valid for interpreting only the structure between 350- and 700-km depths because the rest of the images consists of parts of the RFs that sample areas further than 100 km away from the profiles and are contaminated by crustal multiples (Text S2). Most of the profiles includes more than 1,500 RFs (from 10°E to 26°E every 1° and from 59°N to 69°N every 0.5°), which ensures high data density, necessary for efficient stacking to suppress noise and reveal coherent signals associated with the structure.

To obtain maps of the depth to interfaces and estimate the uncertainty, the chosen set of the RFs was bootstrap resampled with replacement (Efron & Tibshirani, 1991). We subsequently applied automatic picking of the maximum amplitude in target depth windows (±50 km) around the 410 and 660 (Hier-Majumder & Tauzin, 2017). By this procedure, we obtain depth distributions with uncertainty estimates taken as one standard deviation of the distribution. To reconstruct the three-dimensional depth variations of the 410 and 660, we used an average depth value from four adjacent profiles to each 55 × 55-km cell in the grid to build the resulting maps (Tauzin et al., 2013).

The applied methodology implies that all the obtained values of depths to the 410 and 660 should be interpreted relative to the velocity model used for time-to-depth migration (1-D IASP91 and 3-D ZHU15 in our case). The velocity structure of the UM above the MTZ influences the observed depth to each discontinuity (Chevrot et al., 1999). It is possible to subtract this influence by building maps of MTZ thickness variations that are only affected by the pressure/temperature dependence of phase changes and velocity variations within the MTZ. Maps of the 410 and 660 were built for the same set of RFs based on piercing points locations at 535-km depth in the middle of the MTZ (Kosarev et al., 2018). We consequently subtracted the two 410 and 660 maps to obtain the thickness of the MTZ. The uncertainty on the transition zone thickness is calculated as the square root of the sum of the squared uncertainty values for the 410 and 660. Only the results within the low uncertainty area ($1\sigma < 15$ km) are discussed. We provide an extended Method section in the supporting information.

3. Results

The converted signals for both the 410 and 660 discontinuities are clearly visible on all the network stacks (Figure S3), which indicate that the data recorded by each individual network contain reliable information about the MTZ (Figure S3). Using these data, we obtain CCP stacks over a region between 4–34°E and 55–73°N with profiles arranged as a mesh of ~55 by 55 km (Figure 2) and two sets of MTZ maps using the IASP91 and ZHU15 models for migration. Each set of maps includes the depth to the 410 and 660 and the thickness of the MTZ, with uncertainties (Figures 3, S4, and S5). We discuss these observations with respect to the reference values of 410- and 660-km depths and 250-km MTZ thickness, from the IASP91 model.

The obtained CCP stacked profiles include pronounced converted signals at depths around 410 and 660 km (Figures 2 and S2). The amplitude of the conversion at the 660 is slightly smaller than at the 410, on average 0.48% against 0.59%, especially on the profiles west of 10°E, east of 26°E, south of 59°N, and north of 69°N with lower data density (Figures 1c and S6). The best quality CCP stacks are obtained between 10–26°E and 59–69°N, which is the area with the highest data density that ensures the smallest uncertainties (<15 km) for the maps (Figures S4 and S5).

Our maps (Figures 3a–3c) calculated from time-to-depth migration in IASP91 show that the depths to the 410 and 660 are positively correlated (+0.53 Pearson correlation coefficient for depth estimates with uncertainty <15 km; Figure S7e) and elevated above standard values (Figures 3a and 3b). The observed 410 and 660 appear to be up to 15 and 20 km, respectively, shallower than standard (Figures 3a and 3b). The mean depths are 403.5 and 648 km with standard deviations ±14 and ±11 km in the study region respectively (Figure S7). Both discontinuities are imaged relatively deep in western Fennoscandia, beneath Norway, with depths reaching reference values (410 and 660 km; Figures 3a–3c). In the central part of Fennoscandia, approximately beneath Sweden, the discontinuities are up to 15 and 20 km shallower than standard values. To the east in southern Finland, both the 410 and 660 are deeper with standard values for the 410 and 10 km shallower than standard depth for the 660. The MTZ is generally slightly thinner than standard with a mean around 244 km and standard deviation ±9 km over the region (Figure 3c) and overall variations between 220 and 265 km.

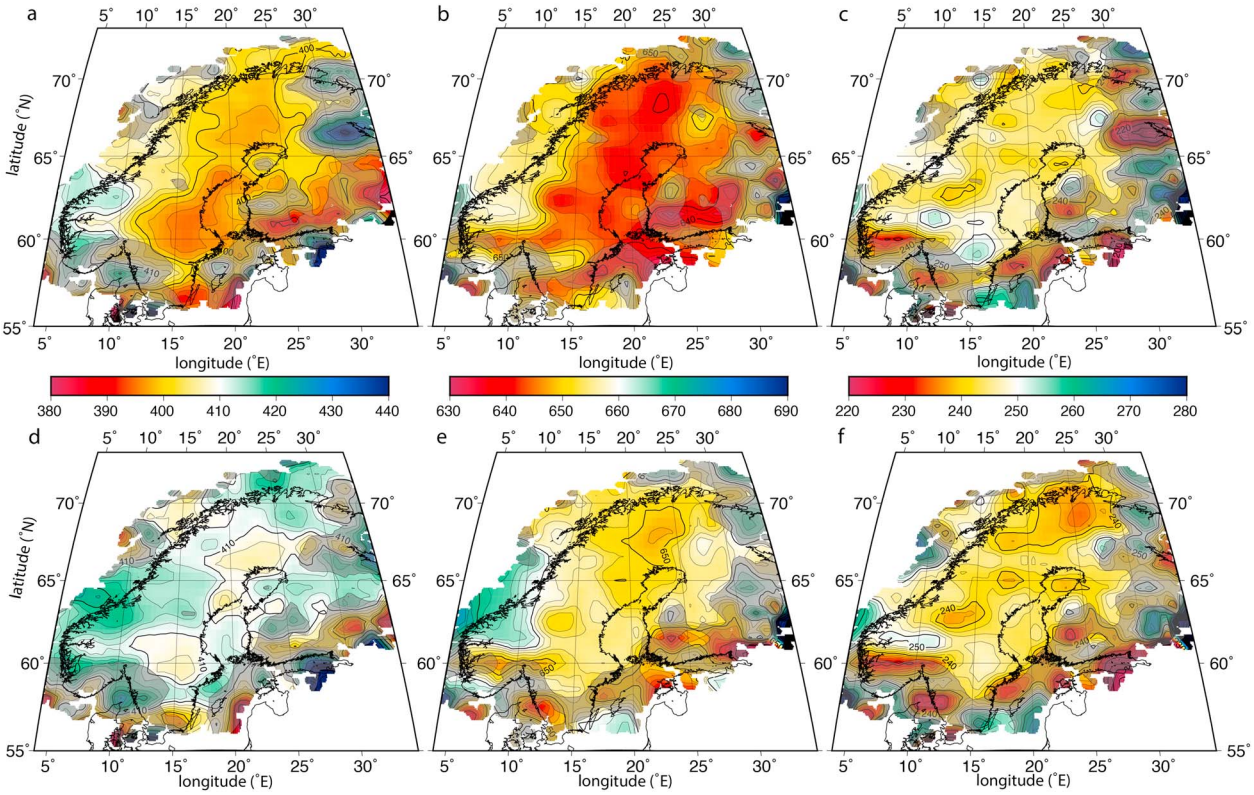

Figure 3. Maps of the depth to the 410- (a, d), 660-km (b, e) discontinuities and the thickness of the mantle transition zone (c, f) obtained using the IASP91 velocity model (Kennett & Engdahl, 1991) in the upper row and the ZHU15 velocity model (Zhu et al., 2015) in the lower row. The regional ZHU15 model provides a more realistic estimate of velocities, therefore the results in the bottom row are considered more reliable than in the upper row. The figure thus demonstrates the bias that may be introduced in studies using the general IASP91 model for time to depth migration. The light gray transparent shading covers areas with uncertainty larger than 15 km for (a, b), and 20 km for (c). White color covers areas without data.

Corrected for the UM structure with the ZHU15 velocity model (Figures 3d–3f), the depths to the 410 and 660 are close to reference values (Figures S7a–S7c) and the Pearson correlation coefficient for depth estimates is only +0.08 (Figure S7d). However, the general relief remains—both the 410 and 660 are slightly deeper in the west and east than in the central part. The depth to the 410 is close to reference (413 km with ±13 km standard deviation over the region; Figures 3d and S7a). The 660 is shallower with an average value of 656 km with standard deviation ±13 km over the region, but the difference can locally reach 15 km. The thickness of the MTZ generally varies from 235 to 255 km and is overall thinner than the 250-km reference by 5–10 km. The mean value for the MTZ thickness is 242 km with a spatial variation of 12 km (Figures 3f and S7c).

The MTZ appears slightly thinner than normal (8–15 km) in the central part of the study area (Figure 3f). MTZ has standard thickness in Southern Norway along 62°N, in the north at 68°N and 14°E and in Finland 63°N, 24°E and 67°N, 27°E. The latter two locations are close to the high uncertainty area in Figure 3. Areas with high uncertainty are characterized by short-wavelength variation in thickness (Figure S5c): the area in southern Norway with thickness of 230 km is adjacent to an area with standard thickness; in Finland several small areas with thickness of 255 km are surrounded by an area with average 245-km thickness. Patchy anomalies in Finland spatially correlate with the Archaean part and its transition to the Proterozoic part of the Baltic Shield. Here the MTZ locally reaches 265 km in thickness with high observational uncertainties, as indicated by the mask in gray (Figure 3f).

Faint neutral-to-positive amplitude signals in the mid-MTZ on CCP stack images could indicate the presence of the 520-km discontinuity (Figures 2 and S2). This interface is often attributed to the wadsleyite-to-ringwoodite mineral transition (Shearer, 1996). Although the idea of the existence of the 520-km discontinuity was challenged by Bock (1994), there is now a large consensus on its existence (e.g., Lawrence & Shearer,

2006b). The increase in seismic velocities across the discontinuity at 520-km depth is usually weak, potentially explaining the poor imaging with RFs.

Other peculiar features observed in the CCP images are localized negative amplitudes (Figure 2 and S2) gathered above the 410 in the northern part of our maps (within the area 16–25°E 67–68°N, centered around 23°E 67°N). It may indicate the presence of a LVZ below ~350-km depth (Revenaugh & Sipkin, 1994; Tauzin et al., 2010; Thybo et al., 2003; Vinnik & Farra, 2007). We also observe negative amplitudes within the MTZ, right above the 660 in the area of Gulf of Bothnia (16–21°E 61–62°N), which might be an indication of the presence of a 590-km discontinuity (Figures 2 and S2; Shen et al., 2014; Tauzin et al., 2013).

4. Discussion

4.1. Effect of Shallow UM Velocities on Depth Maps

Our results support the conclusion of previous studies revealing high seismic velocities in the Fennoscandian UM compared to IASP91 (Alinaghi et al., 2003; Bock et al., 2001; Kozlovskaya et al., 2008; Olsson et al., 2007; Vinnik et al., 2016). Both the 410 and 660 are uplifted by up to 15 km for the 410 and 20 km for the 660 relative to standard values for time-to-depth migration with the IASP91 model (Figures 3a–3c, S2, and S7). Such depth differences could in principle be explained by thermal variation, with reversed cold and hot temperatures in the vicinity of the 410 and 660, respectively. However, several lines of evidence suggest that these are not related to thermal variations around the MTZ but instead to higher velocity in the UM in Scandinavia than in IASP91:

(i) Shallow UM velocity heterogeneities affect the 410 and 660 in the same way; that is, both interfaces appear deeper than expected in case of a slow UM and shallower than expected in the case of a fast UM. Here, the topography of the 410 and 660 are positively correlated (Figures S7d and S7e). In particular, both interfaces are deep in the western Fennoscandia (Figures 3a and 3b). A slightly similar pattern remains after correction using the ZHU15 model (Figures 3d and 3e).

(ii) Ideally, if the UM effects are correctly removed by use of a reliable 3-D velocity model (ZHU15), the points on the correlation plot of the 410 and 660 topography would concentrate around standard values. This occurs when we correct for the 3-D structure using the ZHU15 model (Figures S7d and S7e): The points form a tighter cloud near standard values for the 410 and 660 depths, and the Pearson correlation coefficient between topographies decreases from +0.53 to +0.08, indicating at least partial removal of the UM effects.

(iii) Further, (1) the depth distribution for the 410 interface becomes narrower, (2) the uncertainties are reduced (Figures S4, S5, and S7), (3) stacked amplitudes increase, and (4) the spatial continuity of interfaces on the CCP images improves with the ZHU15 model instead of IASP91 (Figures 2 and S2). These results are caused by better focusing of the converted seismic signals in the depth domain before stacking. In particular before correction, the distribution of 660 depths is bimodal, with maxima centered at 643- and 652-km depths (Figure S7b). After correction using the ZHU15 model, the distribution is unimodal centered around 655 km (Figure S7b). Similar, but less pronounced effect is observed for the depth distribution to the 410 (Figure S7a).

The amplitudes of conversion at the 410 and 660 are the smallest for the networks deployed in Finland (networks ZB and XK in Figure S3). It is also the area with the highest uncertainties in our maps (Figures S4 and S5). Factors explaining this may include the following: (i) lower density of data—short temporary deployments do not provide sufficient coverage despite a relatively small spacing between stations, (ii) possible complex crustal and UM structure with shallow discontinuities in the crust and structures related to Proterozoic/Archean suture zones unaccounted for in the velocity model (Kozlovskaya et al., 2008; Yliniemia et al., 2004), (iii) strong variations in the local topography of MTZ interfaces, and (iv) extended (>50 km) velocity gradients that decrease conversion amplitudes.

The ZHU15 model is a more accurate representation of the deep velocity structure in Scandinavia than IASP91. As both interfaces have been mapped close to standard depths, it is likely that most of the shear wave velocity variations have been accounted for, including the sharp velocity difference in the UM below Southern Norway and Sweden (up to 0.25 km/s in Vs; Kolstrup & Maupin, 2013; Maupin et al., 2013). The mean value of MTZ thickness (242 km with standard deviation over the area ± 12 km) is close to the standard value of 250 km.

There is a trade-off between shear wave speed and recovered discontinuity depth. Additionally, corrections for 3-D mantle structure are not always accurate. To investigate how our results depend on the chosen model, we have compared the shear velocity structure in the 3-D models ZHU15 and in NA-IP (North Atlantic-Instantaneous Phase) model by Rickers et al. (2013). Locally, differences can be significant (up to 0.15 km/s, that is, $\Delta V \approx 2.5\%$ that corresponds to 13.6-km change in the MTZ thickness; Figure S8a) but the areas with the largest differences coincide with areas with ~15-km uncertainty in our MTZ topography maps. However, the overall difference remains small in the investigated region, with an average of ~0.035 km/s (Figures S8b and S8c) in the MTZ (i.e., $\Delta Vs \approx 0.6\%$). This shear velocity perturbation roughly corresponds to ~3-km difference in thickness (Figure S8a). Thus, correcting using the NA-IP model would not affect our interpretation.

4.2. No Deep Thermal Origin for the High Topography of Scandinavia

One of the most disputed topics in Scandinavia is the cause of the high topography in the Scandinavian mountains with >1,500-m elevation in the southern and northern domes. One of the proposed explanations is lateral influence of the Icelandic plume. Tomographic studies suggest that the UM shear wave velocities are much higher in Sweden than in southern Norway at 100- to 150-km depth (Kolstrup & Maupin, 2013; Maupin et al., 2013). The NA-IP tomography model includes a structure at 100- to 200-km depth beneath southern Norway that have been interpreted as an Icelandic "plume finger" (Schoonman et al., 2017). However, due to resolution issues, there is no unambiguous observation that constrains the maximum depth of these anomalies, and whether they affect mineralogical phase changes. The minimum thermal perturbation detectable by our method is ~30 K (it would create variation in thickness of >5 km that exceeds mean uncertainty). We find standard thickness of the MTZ and almost equally elevated 410 and 660, independent of the UM velocity model. Therefore, it is unlikely that the temperatures causing the low velocities in the sub-Moho mantle extend to the depths of the MTZ.

The crust is thin in southern Norway and it lacks a high-velocity lower crust. This has been explained by lithospheric root delamination (Abramovitz & Thybo, 2000; Artemieva & Meissner, 2012; Frassetto & Thybo, 2013), which might have affected the MTZ. The relatively thin crust is enigmatic as it is observed below the highest topography in Scandinavia, such that isostasy would predict low topography. It has been hypothesized that the Caledonian orogen around 400 Ma was comparable in size and crustal thickness to the Himalayas (Gee, 2015), with a layered structure in the UM (Kind et al., 2013). The lower crust has potentially transformed into eclogite facies, and its increased density may have led to instability of the lithospheric root followed by delamination (Artemieva & Meissner, 2012; Mengel & Kern, 1992). Such piece of a lithosphere would sink through the UM and could potentially reach the MTZ and perturb the temperature field. The MTZ structure resolved by our method has a resolution of ~150 km laterally and 15 km vertically. Within this resolution, our results show no evidence for the presence of lithospheric keel around the MTZ. This does not represent a final rejection of the delamination model, as the keel could be stalled in the upper or lower mantle, or the plate could have moved away from it since delamination.

Another feature that could potentially complicate the MTZ structure in Scandinavia are paleosubducted slabs from the Proterozoic accretion of the Baltica plate (dashed black lines in Figure 1b) and the closure of the Iapetus Ocean. Several seismic studies have reported presence of dipping mantle reflectors below the crust in the Gulf of Bothnia and in the North Sea south of Norway (Abramovitz et al., 1997; Abramovitz & Thybo, 2000; BABEL Working Group, 1990; Balling, 2000; MONA LISA Working Group, 1997). Tomographic studies observe dipping features interpreted as possible paleosubduction and delamination (Eken et al., 2008; Zhu et al., 2012a, 2012b). Other evidence for ancient subducted slabs could be reduction of seismic velocities atop the 410- and 660-km discontinuities and within the MTZ (Revenaugh & Sipkin, 1994; Shen & Blum, 2003). Our CCP stacks contain negative amplitude converters atop the 410 and 660 in a broad region, including the area adjacent to the boundary between the Archean and Proterozoic domains, which might indicate the presence of remnants of paleo subduction. Other possible explanation for the negative conversion atop MTZ are variation in the Mg# or influence of the pyroxene to majorite phase transformation (Thybo et al., 2003).

Although with large uncertainty, relatively thick MTZ is observed in the Archaean parts of the study area, which appear 20–30 km thicker than in the Proterozoic and Caledonian parts of Fennoscandia. MTZ thicknesses of 270–280 km in the northeastern, Archaean part of the East European Craton, and ~240 km in the

Proterozoic part have been observed from travel time analysis of refracted arrivals from the 410 and 660 by Świeczak and Grad (2004). Gao and Liu (2014) observed a relatively thick (>260 km) MTZ in most of the cratonic parts of United States as compared to normal (245–250 km) thickness of the MTZ around the craton. We speculate that the thick MTZ below the Archaean parts of Fennoscandia may indicate low temperature that exists due to long-term cooling of the stable region without tectonic events (Artemieva & Mooney, 2001). This interpretation may be supported by the coincidence between the thick MTZ and extremely thick lithosphere (>250 km) in these parts of the Baltic Shield observed by a variety of geophysical, including thermal, seismic, and electromagnetic studies (Artemieva et al., 2006; Artemieva & Thybo, 2008) and from analysis of mantle xenoliths brought to surface by kimberlitic eruptions (Kukkonen et al., 2003).

5. Conclusion

A large number of RFs form the basis for the first high-resolution maps of the MTZ beneath Fennoscandia, which allow investigation of the topography of the 410 and 660 discontinuities and the MTZ thickness. Our results suggest that the MTZ has a thickness close to reference values (~243 ± 10 km) and that it is not affected by any significant temperature variation in the Proterozoic and Caledonian areas. However, we observe a thicker MTZ (265 km ± 20 km) in the Archaean parts of the shield, which may be the result of long-term stable cooling. Both the 410 and the 660 discontinuities appear to be slightly deeper than normal beneath Norway. We demonstrate that the maps obtained using the 3-D velocity model by ZHU15 are more accurate than the ones calculated by using the 1-D IASP91 model. We find no evidence in the MTZ beneath Fennoscandia for a deep thermal anomaly that could explain the unusually high topography. The cause of the enigmatic high topography must therefore be found in the shallower structure.

Acknowledgments

We thank Hejun Zhu for discussions about ZHU15 model used in the study and Florian Rickers and Andreas Fichtner for communication and discussion regarding NA-IP model. We are grateful to Stephen S. Gao and an anonymous reviewer for constructive comments that contributed to improve the manuscript. The following institutions have contributed to the operation of the ScanArray and made this study possible: University of Copenhagen, University of Oslo, University of Aarhus, GeoForschungsZentrum Potsdam (GFZ), and Karlsruhe Institute of Technology (KIT). Closely related networks contributing to ScanArray are NEONOR2 (University of Bergen and NORSAR), the Norwegian National Seismic Network (University of Bergen), seismic array stations in Norway (NORSAR), and the Swedish SNSN network. This study received financial support from DFF (Independent Research Fund Denmark) grant FNU-16/059776-15 to Hans Thybo from which the PhD study of A. M. is financed. B. T. has received funding from the European Union's Horizon 2020 research and innovation program under the Marie Sklodowska-Curie grant agreement 793824. Geological map is digitized using Didger, 2017, by Franz Lutz and Michael Grund at KIT Karlsruhe. The data for this study were requested using ObsPy (Krischer et al., 2015) from the following sources: Data from ScanArray Core (1G) will be publicly available by the end of 2019 though the GEOFON; data from ScanLips I (YF), II (Y1), and 3-D (ZS) are available via IRIS and University of Leicester (SEIS UK); data from Norwegian Seismic Array (NORSAR, NO) and Norwegian National Seismic Network are available via ORFEUS; data from LAPNET/POLENET (XK; Kozlovskaya, 2007) are available via RESIF; NEONOR2 (2-D), Finnish permanent stations (HE), SVEKALAPKO (ZB; Bock et al., 2001) and CENMOVE (ZS; Svenningsen et al., 2007); data are available at GEOFON archive; data from MAGNUS broadband stations (Z6; Weidle et al., 2010) are available at KIT archive.

References

Abramovitz, T., Berthelsen, A., & Thybo, H. (1997). Proterozoic sutures and terranes in the southeastern Baltic Shield interpreted from BABEL deep seismic data. *Tectonophysics*, *270*(3–4), 259–277. https://doi.org/10.1016/S0040-1951(96)00213-2

Abramovitz, T., & Thybo, H. (2000). Seismic images of Caledonian, lithosphere-scale collision structures in the southeastern North Sea along Mona Lisa Profile 2. *Tectonophysics*, *317*(1–2), 27–54. https://doi.org/10.1016/S0040-1951(99)00266-8

Alinaghi, A., Bock, G., Kind, R., Hanka, W., & Wylegalla, K. (2003). Receiver function analysis of the crust and upper mantle from the North German Basin to the Archaean Baltic Shield. *Geophysical Journal International*, *155*(2), 641–652. https://doi.org/10.1046/j.1365-246X.2003.02075.x

Anell, I., Thybo, H., & Artemieva, I. M. (2009). Cenozoic uplift and subsidence in the North Atlantic region: Geological evidence revisited. *Tectonophysics*, *474*(1–2), 78–105. https://doi.org/10.1016/j.tecto.2009.04.006

Anell, I., Thybo, H., & Rasmussen, E. (2012). A synthesis of Cenozoic sedimentation in the North Sea. *Basin Research*, *24*(2), 154–179. https://doi.org/10.1111/j.1365-2117.2011.00517.x

Anell, I., Thybo, H., & Stratford, W. (2010). Relating Cenozoic North Sea sediments to topography in southern Norway: The interplay between tectonics and climate. *Earth and Planetary Science Letters*, *300*(1–2), 19–32. https://doi.org/10.1016/j.epsl.2010.09.009

Artemieva, I. M., & Meissner, R. (2012). Crustal thickness controlled by plate tectonics: A review of crust-mantle interaction processes illustrated by European examples. *Tectonophysics*. Elsevier, *530-531*, 18–49. https://doi.org/10.1016/j.tecto.2011.12.037

Artemieva, I. M., & Mooney, W. D. (2001). Thermal thickness and evolution of Precambrian lithosphere: A global study. *Journal of Geophysical Research*, *106*(B8), 16,387–16,414. https://doi.org/10.1029/2000JB900439

Artemieva, I. M., & Thybo, H. (2008). Deep Norden: Highlights of the lithospheric structure of Northern Europe, Iceland, and Greenland. *Episodes*, *31*(March), 98–106.

Artemieva, I. M., Thybo, H., & Kaban, M. K. (2006). Deep Europe today: Geophysical synthesis of the upper mantle structure and lithospheric processes over 3.5 Ga. *Geological Society, London, Memoirs*, *32*(1), 11–41. https://doi.org/10.1144/GSL.MEM.2006.032.01.02

BABEL Working Group (1990). Evidence for early proterozoic plate tectonics from seismic reflection profiles in the Baltic Shield. *Nature*, *348*(6296), 34–38. https://doi.org/10.1038/348034a0

Balling, N. (2000). Deep seismic reflection evidence for ancient subduction and collision zones within the continental lithosphere of northwestern Europe. *Tectonophysics*, *329*(1–4), 269–300. https://doi.org/10.1016/S0040-1951(00)00199-2

Bercovici, D., & Karato, S. (2003). Whole-mantle convection and the transition-zone water filter. *Nature*, *425*(6953), 39–44. https://doi.org/10.1038/nature01918

Bina, C. R., & Helffrich, G. (1994). Phase transition Clapeyron slopes and transition zone seismic discontinuity topography. *Journal of Geophysical Research*, *99*(B8), 15853. https://doi.org/10.1029/94JB00462

Bock, G. (1994). Synthetic seismogram images of upper mantle structure: No evidence for a 520-km discontinuity. *Journal of Geophysical Research*, *99*(B8), 15843. https://doi.org/10.1029/94JB00992

Bock, G., Achauer, U., Alinaghi, A., Ansorge, J., Bruneton, M., Friederich, W., et al. (2001). Seismic probing of Fennoscandian lithosphere. *Eos*, *82*(50), 621–629. https://doi.org/10.1029/01EO00356

Bostock, M. G. (1999). Seismic waves converted from velocity gradient anomalies in the Earth's upper mantle. *Geophysical Journal International*, *138*(3), 747–756. https://doi.org/10.1046/j.1365-246X.1999.00902.x

Chevrot, S., Vinnik, L., & Montagner, J.-P. (1999). Global-scale analysis of the mantle *Pds* phases. *Journal of Geophysical Research*, *104*(B9), 20,203–20,219. https://doi.org/10.1029/1999JB900087

Dueker, K. G., & Sheehan, A. F. (1997). Mantle discontinuity structure from midpoint stacks of converted *P* to *S* waves across the Yellowstone hotspot track. *Journal of Geophysical Research*, *102*(B4), 8313–8327. https://doi.org/10.1029/96JB03857

Efron, B., & Tibshirani, R. (1991). Statistical data analysis in the computer age. *Science*, *253*(5018), 390–395. https://doi.org/10.1126/science.253.5018.390

Eken, T., Shomali, Z. H., Roberts, R., Hieronymus, C. F., & Bodvarsson, R. (2008). S and P velocity heterogeneities within the upper mantle below the Baltic Shield. *Tectonophysics*, *462*(1-4), 109–124. https://doi.org/10.1016/j.tecto.2008.02.015

Foulger, G. R., Panza, G. F., Artemieva, I. M., Bastow, I. D., Cammarano, F., Evans, J. R., et al. (2013). Caveats on tomographic images. *Terra Nova*, *25*(4), 259–281. https://doi.org/10.1111/ter.12041

Frassetto, A., & Thybo, H. (2013). Receiver function analysis of the crust and upper mantle in Fennoscandia—Isostatic implications. *Earth and Planetary Science Letters*, *381*, 234–246. https://doi.org/10.1016/j.epsl.2013.07.001

Frost, D. J. (2003). The structure and sharpness of $(Mg,Fe)_2SiO_4$ phase transformations in the transition zone. *Earth and Planetary Science Letters*, *216*(3), 313–328. https://doi.org/10.1016/S0012-821X(03)00533-8

Gabrielsen, R. H., Faleide, J. I., Pascal, C., Braathen, A., Nystuen, J. P., Etzelmuller, B., & O'Donnell, S. (2010). Latest Caledonian to present tectonomorphological development of southern Norway. *Marine and Petroleum Geology*, *27*(3), 709–723. https://doi.org/10.1016/j.marpetgeo.2009.06.004

Gao, S. S., & Liu, K. H. (2014). Mantle transition zone discontinuities beneath the contiguous United States. *Journal of Geophysical Research: Solid Earth.*, *119*, 6452–6468. https://doi.org/10.1002/2014JB011253

Gee, D. G., Fossen, H., Henriksen, N., & Higgins, A. K. (2008). From the early Paleozoic platforms of Baltica and Laurentia to the Caledonide orogen of Scandinavia and Greenland. *Episodes*, *31*, 44–51.

Gee, D. G. (2015). Caledonides of Scandinavia, Greenland, and Svalbard☆. In *Reference module in Earth systems and Environmental Sciences* (pp. 1–15). Elsevier. https://doi.org/10.1016/B978-0-12-409548-9.09133-8

Hier-Majumder, S., & Tauzin, B. (2017). Pervasive upper mantle melting beneath the western US. *Earth and Planetary Science Letters*, *463*, 25–35. https://doi.org/10.1016/j.epsl.2016.12.041

Högdahl, K., Andersson, U. B., Eklund, O., Karin, H., Gorbatschev, R., Nystr, J. et al. (2004). The Trans Scandinavian Igneous Belt (TIP) in Sweden: A review of its character and evolution. Geological Survey of Finland (Vol. 37).

Irifune, T. (1987). An experimental investigation of the pyroxene-garnet transformation in a pyrolite composition and its bearing on the constitution of the mantle. *Physics of the Earth and Planetary Interiors*, *45*(4), 324–336. https://doi.org/10.1016/0031-9201(87)90040-9

Japsen, P., & Chalmers, J. A. (2000). Neogene uplift and tectonics around the North Atlantic: Overview. *Global and Planetary Change*, *24*(3–4), 165–173. https://doi.org/10.1016/S0921-8181(00)00006-0

Japsen, P., Chalmers, J. A., Green, P. F., & Bonow, J. M. (2012). Elevated, passive continental margins: Not rift shoulders, but expressions of episodic, post-rift burial and exhumation. *Global and Planetary Change*, *90-91*(Supplement C), 73–86. https://doi.org/10.1016/j.gloplacha.2011.05.004

Kennett, B. L. N., & Engdahl, E. R. (1991). Traveltimes for global earthquake location and phase identification. *Geophysical Journal International*, *105*(2), 429–465. https://doi.org/10.1111/j.1365-246X.1991.tb06724.x

Kind, R., Sodoudi, F., Yuan, X., Shomali, H., Roberts, R., Gee, D., et al. (2013). Scandinavia: A former Tibet. *Geochemistry, Geophysics, Geosystems*, *14*, 4479–4487. https://doi.org/10.1002/ggge.20251

Kolstrup, M. L., & Maupin, V. (2013). A Proterozoic boundary in southern Norway revealed by joint-inversion of *P*-receiver functions and surface waves. *Precambrian Research*, *238*, 186–198. https://doi.org/10.1016/j.precamres.2013.10.004

Korja, A., & Heikkinen, P. (2005). The accretionary Svecofennian orogen—Insight from the BABEL profiles. *Precambrian Research*, *136*(3–4), 241–268. https://doi.org/10.1016/j.precamres.2004.10.007

Kosarev, G., Oreshin, S., Vinnik, L., & Makeyeva, L. (2018). Mantle transition zone beneath the central Tien Shan: Lithospheric delamination and mantle plumes. *Tectonophysics*, *723*, 172–177. https://doi.org/10.1016/j.tecto.2017.12.010

Kozlovskaya, E. (2007). Seismic network XK:LAPNET/POLENET seismic temporary array (RESIF-SISMOB). RESIF - Réseau Sismologique et géodésique Français. https://doi.org/10.15778/RESIF.XK2007

Kozlovskaya, E., Kosarev, G., Aleshin, I., Riznichenko, O., & Sanina, I. (2008). Structure and composition of the crust and upper mantle of the Archean-Proterozoic boundary in the Fennoscandian shield obtained by joint inversion of receiver function and surface wave phase velocity of recording of the SVEKALAPKO array. *Geophysical Journal International*, *175*(1), 135–152. https://doi.org/10.1111/j.1365-246X.2008.03876.x

Krischer, L., Megies, T., Barsch, R., Beyreuther, M., Lecocq, T., Caudron, C., & Wassermann, J. (2015). ObsPy: A bridge for seismology into the scientific Python ecosystem. *Computational Science and Discovery*, *8*(1), 14003. https://doi.org/10.1088/1749-4699/8/1/014003

Kukkonen, I. T., Kinnunen, K. A., & Peltonen, P. (2003). Mantle xenoliths and thick lithosphere in the Fennoscandian Shield. *Physics and Chemistry of the Earth*, *28*(9-11), 349–360. https://doi.org/10.1016/S1474-7065(03)00057-3

Langston, C. A. (1979). Structure under Mount Rainier, Washington, inferred from teleseismic body waves. *Journal of Geophysical Research*, *84*(B9), 4749. https://doi.org/10.1029/JB084iB09p04749

Lawrence, J. F., & Shearer, P. M. (2006a). A global study of transition zone thickness using receiver functions. *Journal of Geophysical Research*, *111*, B06307. https://doi.org/10.1029/2005JB003973

Lawrence, J. F., & Shearer, P. M. (2006b). Constraining seismic velocity and density for the mantle transition zone with reflected and transmitted waveforms. *Geochemistry, Geophysics, Geosystems*, *7*, Q10012. https://doi.org/10.1029/2006GC001339

Ligorría, J. P., & Ammon, C. J. (1999). Iterative deconvolution and receiver function estimation. *Bulletin of the Seismological Society of America*, *89*(October), 1395–1400.

Maupin, V., Agostini, A., Artemieva, I., Balling, N., Beekman, F., Ebbing, J., et al. (2013). The deep structure of the Scandes and its relation to tectonic history and present-day topography. *Tectonophysics*, *602*, 15–37. https://doi.org/10.1016/j.tecto.2013.03.010

Medhus, A. B., Balling, N., Jacobsen, B. H., Weidle, C., England, R. W., Kind, R., et al. (2012). Upper-mantle structure beneath the Southern Scandes Mountains and the Northern Tornquist Zone revealed by P-wave traveltime tomography. *Geophysical Journal International*, *189*(3), 1315–1334. https://doi.org/10.1111/j.1365-246X.2012.05449.x

Mengel, K., & Kern, H. (1992). Evolution of the petrological and seismic Moho; Implications for the continental crust-mantle boundary. *Terra Nova*, *4*(1), 109–116. https://doi.org/10.1111/j.1365-3121.1992.tb00455.x

MONA LISA Working Group (1997). MONA LISA—Deep seismic investigations of the lithosphere in the southeastern North Sea. *Tectonophysics*, *269*(1), 1–19.

Nielsen, S. B., Gallagher, K., Leighton, C., Balling, N., Svenningsen, L., Jacobsen, B. H., et al. (2009). The evolution of western Scandinavian topography: A review of Neogene uplift versus the ICE (isostasy-climate-erosion) hypothesis. *Journal of Geodynamics*, *47*(2–3), 72–95. https://doi.org/10.1016/j.jog.2008.09.001

Olsson, S., Roberts, R. G., Shomali, Z. H., & Bödvarsson, R. (2007). Tomographic inversion of P410s delay times for simultaneous determination of *P* and *S* velocities of the upper mantle beneath the Baltic Shield. *Physics of the Earth and Planetary Interiors*, *160*(2), 157–168. https://doi.org/10.1016/j.pepi.2006.11.005

Pedersen, V. K., Huismans, R. S., & Moucha, R. (2016). Isostatic and dynamic support of high topography on a North Atlantic passive margin. *Earth and Planetary Science Letters*, *446*, 1–9. https://doi.org/10.1016/j.epsl.2016.04.019

Revenaugh, J., & Sipkin, S. A. (1994). Seismic evidence for silicate melt atop the 410-km mantle discontinuity. *Nature*, *369*(6480), 474–476. https://doi.org/10.1038/369474a0

Rickers, F., Fichtner, A., & Trampert, J. (2013). The Iceland-Jan Mayen plume system and its impact on mantle dynamics in the North Atlantic region: Evidence from full-waveform inversion. *Earth and Planetary Science Letters*, *367*(Supplement C), 39–51. https://doi.org/10.1016/j.epsl.2013.02.022

Ringwood, A. E. (1969). Phase transformations in the mantle. *Earth and Planetary Science Letters*, *5*, 401–412. https://doi.org/10.1016/S0012-821X(68)80072-X

Schoonman, C. M., White, N. J., & Pritchard, D. (2017). Radial viscous fingering of hot asthenosphere within the Icelandic plume beneath the North Atlantic Ocean. *Earth and Planetary Science Letters*, *468*(Supplement C), 51–61. https://doi.org/10.1016/j.epsl.2017.03.036

Shearer, P. M. (1996). Transition zone velocity gradients and the 520-km discontinuity. *Journal of Geophysical Research*, *101*(B2), 3053–3066. https://doi.org/10.1029/95JB02812

Shen, X., Yuan, X., & Li, X. (2014). A ubiquitous low-velocity layer at the base of the mantle transition zone. *Geophysical Research Letters*, *41*, 836–842. https://doi.org/10.1002/2013GL058918

Shen, Y., & Blum, J. (2003). Seismic evidence for accumulated oceanic crust above the 660-km discontinuity beneath southern Africa. *Geophysical Research Letters.*, *30*(18), 1925. https://doi.org/10.1029/2003GL017991

Svenningsen, L., Balling, N., Jacobsen, B. H., Kind, R., Wylegalla, K., & Schweitzer, J. (2007). Crustal root beneath the highlands of southern Norway resolved by teleseismic receiver functions. *Geophysical Journal International*, *170*(3), 1129–1138. https://doi.org/10.1111/j.1365-246X.2007.03402.x

Świeczak, M., & Grad, M. (2004). Upper mantle seismic discontinuities: Topography variations beneath Eastern Europe. *Acta Geophysica Polonica*, *52*(3), 251–271.

Tauzin, B., Debayle, E., & Wittlinger, G. (2008). The mantle transition zone as seen by global *Pds* phases: No clear evidence for a thin transition zone beneath hotspots. *Journal of Geophysical Research*, *113*, B08309. https://doi.org/10.1029/2007JB005364

Tauzin, B., Debayle, E., & Wittlinger, G. (2010). Seismic evidence for a global low-velocity layer within the Earth's upper mantle. *Nature Geoscience*, *3*(10), 718–721. https://doi.org/10.1038/ngeo969

Tauzin, B., & Ricard, Y. (2014). Seismically deduced thermodynamics phase diagrams for the mantle transition zone. *Earth and Planetary Science Letters*, *401*, 337–346. https://doi.org/10.1016/j.epsl.2014.05.039

Tauzin, B., Van Der Hilst, R. D., Wittlinger, G., & Ricard, Y. (2013). Multiple transition zone seismic discontinuities and low velocity layers below western United States. *Journal of Geophysical Research: Solid Earth*, *118*, 2307–2322. https://doi.org/10.1002/JGRB.50182

Thio, V., Cobden, L., & Trampert, J. (2016). Seismic signature of a hydrous mantle transition zone. *Physics of the Earth and Planetary Interiors*, *250*, 46–63. https://doi.org/10.1016/J.PEPI.2015.11.005

Thybo, H., Balling, N., Maupin, V., Ritter, J., & Tilmann, F. (2012). ScanArray core (1G 2012-2017). https://doi.org/doi:10.14470/6T569239

Thybo, H., Nielsen, L., & Perchuc, E. (2003). Seismic scattering at the top of the mantle transition zone. *Earth and Planetary Science Letters*, *216*(3), 259–269. https://doi.org/10.1016/S0012-821X(03)00485-0

Vinnik, L., & Farra, V. (2007). Low *S* velocity atop the 410-km discontinuity and mantle plumes. *Earth and Planetary Science Letters*, *262*(3–4), 398–412. https://doi.org/10.1016/j.epsl.2007.07.051

Vinnik, L., Kozlovskaya, E., Oreshin, S., Kosarev, G., Piiponen, K., & Silvennoinen, H. (2016). The lithosphere, LAB, LVZ and Lehmann discontinuity under central Fennoscandia from receiver functions. *Tectonophysics*, *667*, 189–198. https://doi.org/10.1016/j.tecto.2015.11.024

Vinnik, L. P. (1977). Detection of waves converted from P to SV in the mantle. *Physics of the Earth and Planetary Interiors*, *15*(1), 39–45. https://doi.org/10.1016/0031-9201(77)90008-5

Wawerzinek, B., Ritter, J. R. R., & Roy, C. (2013). New constraints on the 3D shear wave velocity structure of the upper mantle underneath Southern Scandinavia revealed from non-linear tomography. *Tectonophysics*, *602*, 38–54. https://doi.org/10.1016/j.tecto.2012.12.033

Weidle, C., Maupin, V., Ritter, J., Kvaerna, T., Schweitzer, J., Balling, N., et al. (2010). MAGNUS—A seismological broadband experiment to resolve crustal and upper mantle structure beneath the southern Scandes Mountains in Norway. *Seismological Research Letters*, *81*(1), 76–84. https://doi.org/10.1785/gssrl.81.1.76

Wood, B. J. (1995). The effect of H_2O on the 410-kilometer seismic discontinuity. *Science*, *268*(5207), 74–76. https://doi.org/10.1126/science.268.5207.74

Yliniemia, J., Kozlovskaya, E., Hjelt, S. E., Komminaho, K., & Ushakov, A. (2004). Structure of the crust and uppermost mantle beneath southern Finland revealed by analysis of local events registered by the SVEKALAPKO seismic array: SVEKALAPKO seismic tomography working group. *Tectonophysics*, *394*(1–2), 41–67. https://doi.org/10.1016/j.tecto.2004.07.056

Zhu, H., Bozdağ, E., Peter, D., & Tromp, J. (2012a). Seismic wavespeed images across the Iapetus and Tornquist suture zones. *Geophysical Research Letters*, *39*, L09809. https://doi.org/10.1029/2012GL053053

Zhu, H., Bozdağ, E., Peter, D., & Tromp, J. (2012b). Structure of the European upper mantle revealed by adjoint tomography. *Nature Geoscience*, *5*(7), 493–498. https://doi.org/10.1038/ngeo1501

Zhu, H., Bozdăg, E., & Tromp, J. (2015). Seismic structure of the European upper mantle based on adjoint tomography. *Geophysical Journal International*, *201*(1), 18–52. https://doi.org/10.1093/gji/ggu492

Zhu, L. (2000). Crustal structure across the San Andreas Fault, southern California from teleseismic converted waves. *Earth and Planetary Science Letters*, *179*(1), 183–190. https://doi.org/10.1016/S0012-821X(00)00101-1